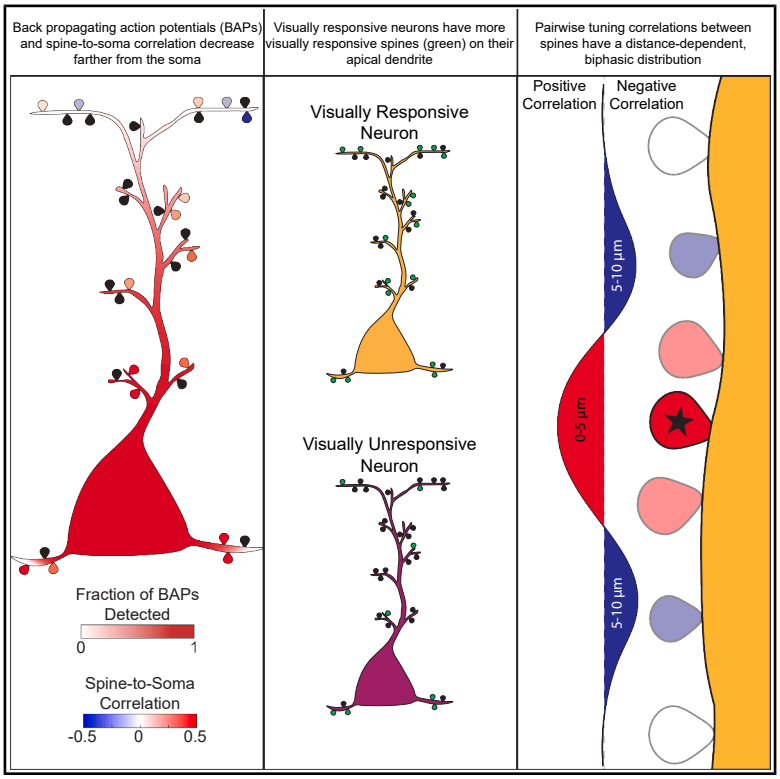
iScience

Article

# Functional organization of dendritic spines in mouse visual cortex layer 2/3 neurons

## Graphical abstract




## Highlights

- Spine-to-soma tuning correlations decrease with distance from the soma
- Responsive neurons have more responsive spines on their apical dendrite
- Spines have distance-dependent organization based on shared tuning
- Spines correlated to the soma are more orientation selective

## Authors

Kyle R. Jenks, Gregg R. Heller, Katya Tsimring, Kendyll B. Martin, Asrah Rizvi, Jacque Pak Kan Ip, Mriganka Sur

## Correspondence

krjenks@mit.edu (K.R.J.), msur@mit.edu (M.S.)

## In brief

Cellular neuroscience; Molecular neuroscience

Jenks et al., 2026, iScience *29*, 115861
June 19, 2026 © 2026 The Author(s). Published by Elsevier Inc.
https://doi.org/10.1016/j.isci.2026.115861

CellPress

iScience

CellPress
OPEN ACCESS

Article

# Functional organization of dendritic spines in mouse visual cortex layer 2/3 neurons

Kyle R. Jenks,[1,*] Gregg R. Heller,[2] Katya Tsimring,[2] Kendyll B. Martin,[2] Asrah Rizvi,[3] Jacque Pak Kan Ip,[4,5] and Mriganka Sur[1,2,6,*]

[1]The Picower Institute for Learning and Memory, Massachusetts Institute of Technology, Cambridge, MA 02139, USA
[2]Department of Brain and Cognitive Sciences, Massachusetts Institute of Technology, Cambridge, MA 02139, USA
[3]Bloomberg School of Public Health, Johns Hopkins University, Baltimore, MD 21205, USA
[4]School of Biomedical Sciences, The Chinese University of Hong Kong, Hong Kong, China
[5]Gerald Choa Neuroscience Institute, The Chinese University of Hong Kong, Hong Kong, China
[6]Lead contact
*Correspondence: krjenks@mit.edu (K.R.J.), msur@mit.edu (M.S.)
https://doi.org/10.1016/j.isci.2026.115861

## SUMMARY

Cortical neurons receive heterogeneous excitatory synaptic inputs, yet the organizational principles underlying their distribution across the dendritic arbor remain poorly understood. Here, we examined how synaptic visual inputs to dendritic spines of mouse visual cortex layer 2/3 excitatory neurons are organized globally and locally using two-photon *in vivo* calcium imaging. In visually responsive neurons, sharply tuned proximal spines showed higher somatic tuning correlation than did distal spines. Responsive neurons had more responsive spines on their apical dendrites and higher pairwise tuning correlations between spines than did unresponsive neurons. While pairwise tuning correlations between spines did not vary significantly with their distance from the soma, spines on responsive neurons were locally clustered based on correlated tuning. Our findings reveal that visual input is not randomly distributed but organized globally and locally in relation to factors including correlation to and distance from the soma as well as correlation to neighboring spines.

## INTRODUCTION

The brain's ability to extract meaningful features from sensory input, such as orientation and direction in the visual cortex (V1), relies heavily on the complex computational capabilities of pyramidal neurons that integrate thousands of excitatory synaptic inputs.[1] The loci of excitatory synaptic input are a neuron's dendritic spines, the formation and elimination of which may be regulated globally by the correlation between presynaptic activity and postsynaptic action potentials and locally by correlated activation of neighboring spines.[2–5] The interplay of global and local factors putatively shapes the resultant organization of excitatory inputs across a pyramidal neuron's dendritic arbor. However, which specific global and local plasticity rules govern individual dendritic spines remain unclear. This could be because these rules are not constant but instead highly compartmentalized, depending critically on a given spine's location in the dendritic arbor, distance from the soma, and distance from other spines on the dendrite.

The orientation preference of mouse V1 layer 2/3 pyramidal neurons reflects the summed and thresholded orientation-responsive inputs to their spines as measured through calcium activity,[2,6] suggesting a biased distribution of synaptic input sharing the soma's preferred stimulus. Indeed, in V1, a like-to-like connectivity bias between responsive neurons exists based on shared visual tuning[7–9] and emerges during development putatively through synaptic plasticity.[5,10] Strengthening or retention of dendritic spines with inputs matching the soma could occur through spike-timing dependent plasticity driven by back propagating action potentials (BAPs) activating synaptic NMDA receptors. However, recent work from the mouse motor cortex suggests a branch-type-specific dichotomy: Dendritic spine potentiation on basal branches is predicted by coincident activity with postsynaptic action potentials, whereas dendritic spine potentiation on apical branches is predicted by local co-activity with neighboring synapses.[11] This distinction implies that basal spines may be biased toward inputs matching the soma, whereas apical spines are more organized locally into co-active clusters.[12,13]

In addition to compartment-specific plasticity rules, distance from the soma could independently impact excitatory synapse organization. The efficacy of synaptic input transmitted to the soma is fundamentally influenced by the spine's distance from the soma, decreasing with increasing distance.[14] Similarly, the somatic output, in the form of BAPs, propagated back into the dendritic arbor attenuates and temporally broadens as it travels,[15–17] although the rate of attenuation can differ by branch type.[18,19] This suggests that spines proximal to the soma are more influenced by somatic output, which could lead to greater homogeneity through biased tuning to the soma's preferred stimulus, while more distal spines receiving weaker somatic feedback may instead rely on local NMDA-dependent calcium spikes driven by co-activity.[4,20]


This is an open access article under the CC BY-NC-ND license (http://creativecommons.org/licenses/by-nc-nd/4.0/).

Moreover, proximity itself contrains synaptic organization, as a dendritic spine can only form synapses with adjacent presynaptic partners. This distribution is not uniform across a neuron's dendritic arbor, as potential presynaptic partners vary vertically as a function of cortical layer and horizontally as a function of retinotopic location.[21–24] Therefore, even in the absence of visually tuned postsynaptic activity, organization of synaptic input may already be established by dendritic morphology and axonal innervation patterns.

Somatic feedback (putatively from BAPs), the intrinsic differences between apical and basal dendritic branches, distance from the soma, and distance between spines themselves can each bias the formation and retention of individual dendritic spines based on their functional properties. While many studies have explored these elements in isolation, a comprehensive understanding of how they collectively correlate to the visual tuning of synapses is incomplete. We set out to map how visually tuned somatic feedback, dendritic branch type, distance between spines, and distance from the soma correlate with dendritic spine responses using two-photon calcium imaging of layer 2/3 pyramidal neurons in mouse V1.

## RESULTS

### Somatic responses reflect the summed activity of dendritic spines

To measure the visually driven activity of both excitatory neurons and their dendritic spines, we sparsely labeled excitatory neurons in mouse V1 by co-injecting a high titer of an AAV containing floxed mRuby2 (red structural marker) and GCaMP6s (green calcium indicator) driven by the synapsin promoter, and a low titer of an AAV containing Cre driven by the CaMKII promoter in layer 2/3 (Figure 1A). The activity of the soma and spines from multiple segments of the dendritic arbor (Figure 1B) was separately measured while awake mice viewed sinusoidal gratings drifting at 2 Hz in multiple directions spaced 22.5–45° apart (Table 1). As each neuron had the same stimulus set used for recording its spine and soma responses, we could compare these responses directly within each neuron to correlate spine and soma visual tuning.

We split recorded neurons into a population responsive to the presented stimuli, whose spines putatively received visually tuned somatic feedback, and a population of unresponsive neurons, whose spines putatively did not receive visually tuned somatic feedback, for the presented stimulus set. As the soma and spines were recorded asynchronously, and BAPs cannot be consistently used as a marker of somatic spiking (as detailed below), we used a ZETA test on the responses of each neuron to its preferred stimulus to ensure that the recorded neuron's responses were robust and stimulus locked across trials.[25] 11 of the 22 recorded neurons were deemed visually responsive to their preferred stimulus (Figure 1C).

There was no significant difference in the density of spines (Figure 1D) or average spine size (Figures 1E and S1) between responsive and unresponsive neurons, suggesting that despite the difference in functional classification, the two groups of neurons had the capacity to receive similar levels of synaptic input. Spine-specific calcium signals were isolated from global (BAPs) and local (NMDA spikes) calcium events as described previously and detailed in the STAR Methods[2,26,27] (Figure 1F). This subtraction effectively removed non-spine-specific calcium signals from dendritic spines (Figure 1G), but seemingly did not overcorrect and remove spine responses occurring during BAPs (and thus correlated to the soma), as the sum of responsive spines' tuning curves mirrored the preference of their parent somata (Figure 1H) as previously reported.[2,6,28] There was no such bias toward any one direction when performing the same alignment for unresponsive neurons (Figure 1I).

### Spine-to-soma correlations decrease with distance from the soma on visually responsive neurons

To determine if the probability of observing a BAP decreased with distance from the soma, and if this decrease was apparent in both apical and basal dendrites,[17,29,30] we compared the number of BAPs recorded across different dendritic segments. As each neuron's level of activity differs, we normalized the number of BAPs recorded from each dendritic segment to the mean number of BAPs taken across all segments for that neuron. We found that within the same neuron, the number of detected BAPs significantly decreased with distance from the soma (Figure 2A) and that there were fewer BAPs detected in apical segments than in basal segments (Figure 2B). However, apical segments were significantly farther from the soma, on average, than basal segments ($F(245) = 108.83$, $p = 2.5*10^{-21}$, ANOVA). Therefore, we analyzed the effect of distance from soma separately in apical and basal segments and found a significant effect of distance from soma in both branch types (Figure 2C). Additionally, to separate the effects of distance from the soma and branch type, we performed partial correlations for the effect of distance from soma controlling for branch type ($t(15) = -2.60$, $p = 0.02$, one-sample $t$ test) and for the effect of branch type controlling for distance from soma ($t(15) = -0.87$, $p = 0.40$, one-sample $t$ test) which showed a significant effect of distance from soma only. Thus, we conclude that the distance from the soma predicts the frequency of observable BAPs in both branch types (Figure 2D).

Given that BAP calcium decreases in more distal dendrites, we hypothesized that dendritic spines proximal to the soma would have higher tuning correlation to the soma than more distal spines. Responsive spines on responsive neurons had variable tuning correlation to their parent soma, but as expected this correlation was, on average, higher than on unresponsive somata (which had a mean spine-to-soma correlation near 0) (Figure 2E). The mean spine-to-soma correlation of spines on responsive neurons' apical and basal branches was not significantly different (Figure 2F). On the other hand, spine-to-soma correlation decreased with increasing distance from the soma (Figure 2G) and the partial correlation between spine-to-soma correlation and distance from soma (controlling for branch type) for responsive neurons was significant and negative (Figure 2H). Thus, both BAPs and spine-to-soma correlation decrease further from the soma.

### Neurons with visually responsive somata have more visually responsive spines

While spines on a responsive neuron are biased toward the soma's preferred stimulus, does somatic visual responsiveness,

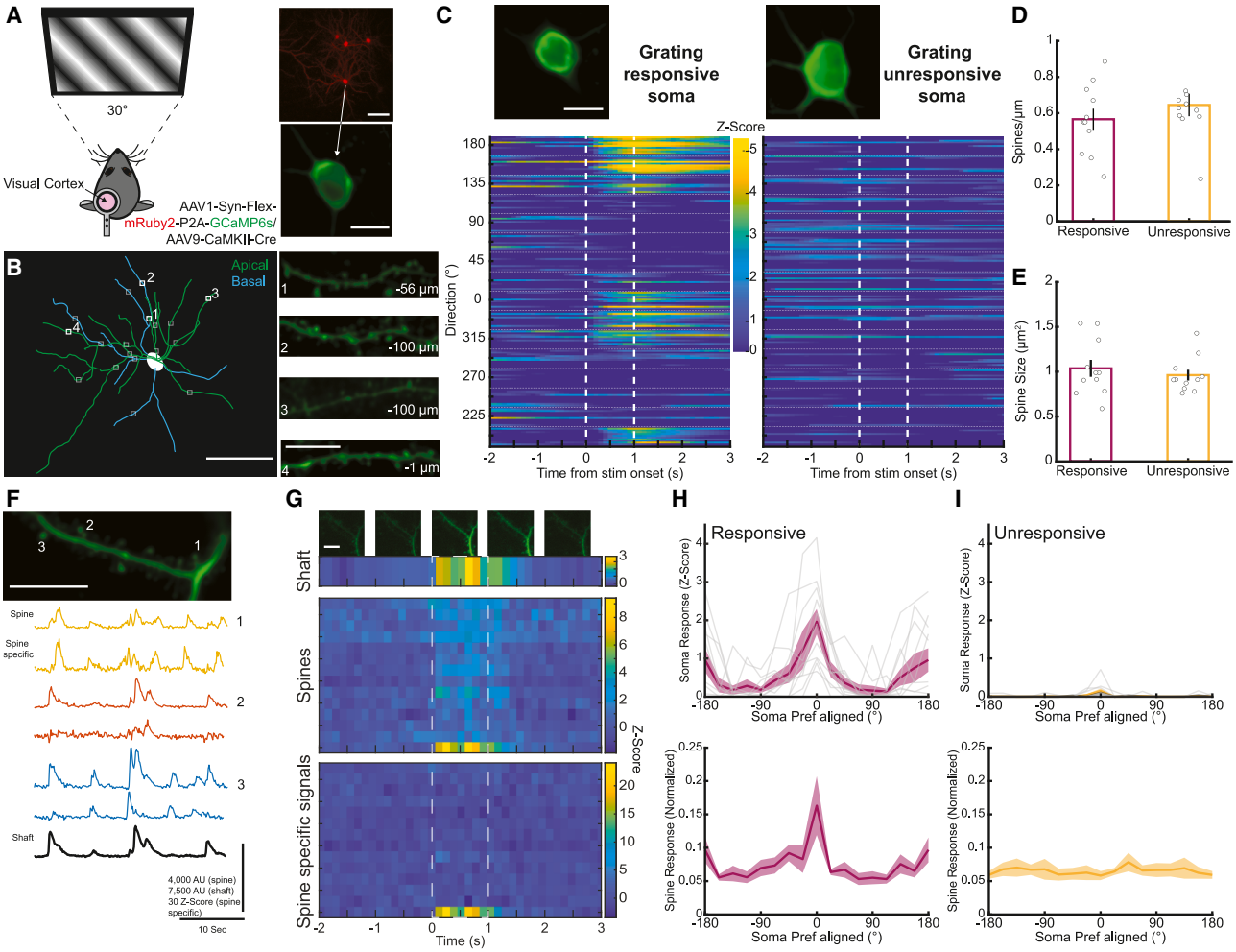



**Figure 1. Somatic responses reflect the summed activity of dendritic spines**

(A) Experimental design. Head-fixed, awake mice viewed drifting grating stimuli on a monitor (left). Excitatory neurons were labeled with the structural marker mRuby2 (right, top. Scale bars, 100 µm) and calcium indicator GCaMP6s (right, bottom. Scale bars, 10 µm).

(B) In addition to imaging of the soma, apical (green) and basal (blue) segments of the dendritic arbor were imaged (left. Boxes indicate imaged regions. Scale bars, 100 µm). Representative imaged segments of dendrites (right. Correspond to white, numbered boxes on left) from apical (1, 4) and basal (2, 3) branches (Depth measured from the highest apical termination. Scale bars, 10 µm).

(C) Stimulus-aligned, z-scored responses of a neuron classified as responsive (left) and a neuron classified as unresponsive (right). Vertical white dashed lines indicate the onset (0 s) and offset (1 s) of each stimulus. Horizontal white dashed lines separate each block of the 10 repetitions of each direction. Stimuli are sorted by direction but were presented in random order (scale bars, 10 µm).

(D) The density of dendritic spines across all imaged dendritic segments averaged per neuron for responsive and unresponsive neurons ($t(20) = -0.92$, $p = 0.37$, *t* test).

(E) Spine size (area) averaged per neuron for responsive and unresponsive neurons ($t(20) = 0.66$, $p = 0.52$, *t* test).

(F) Isolation of spine-specific signals. A representative dendritic segment is shown. The original spine signals are regressed to the signal from the dendritic shaft to isolate the spine-specific signal, which is then z-scored (scale bars, 10 µm).

(G) Example dendritic segment experiencing a back-propagating action potential during a visual stimulus. Fluorescent images before, during, and after the back propagating action potential show calcium activity throughout the shaft and the spines (scale bars, 10 µm). Calcium activity is present throughout the dendritic shaft during the stimulus (top activity trace). Spine signal without removing correlated activity from the shaft (middle traces). Isolation of spine-specific signals (bottom traces). Vertical white dashed lines indicate the onset (0 s) and offset (1 s) of the visual stimulus.

(H) The average tuning curve of all responsive somata (top. Individual neurons shown as light gray lines) and their summed input (bottom), with each soma's tuning curve and that of their input aligned to that soma's preferred direction. The solid line denotes the mean, and the shaded region the standard error.

(I) Same as in H., but for the unresponsive somata. For bar plots, circles show the mean of each neuron, while the bars show the mean of each group. Error bars show the standard error of each group. * denotes a significant effect.

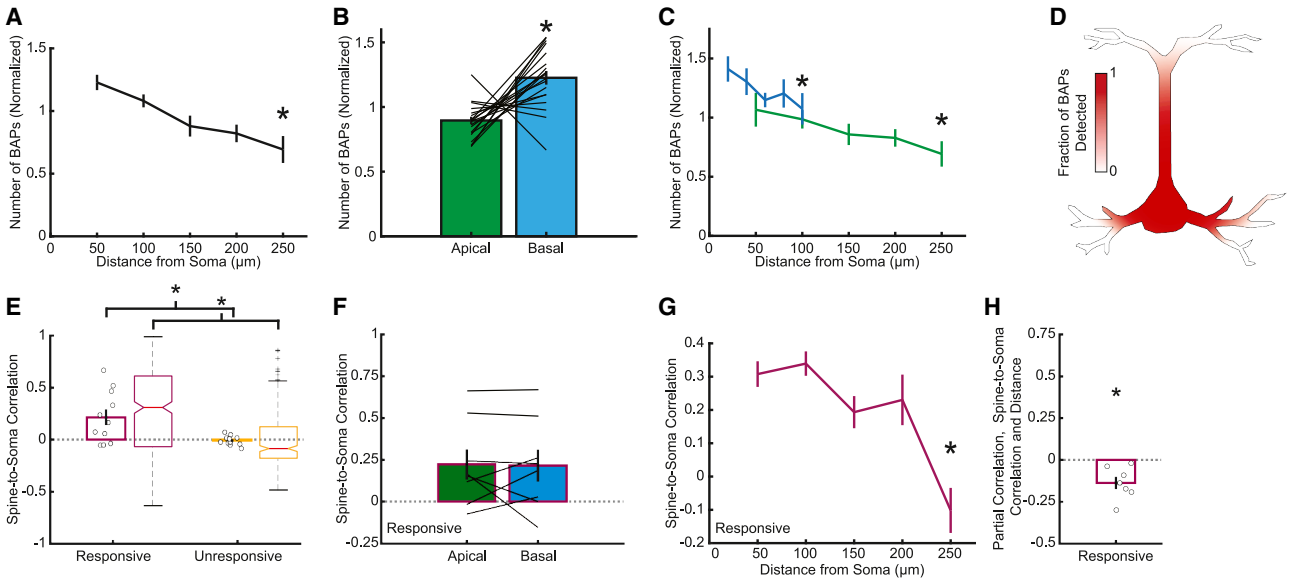



**Figure 2. Spine-to-soma correlations decrease with distance from the soma on visually responsive neurons**

(A) The number of back propagating action potentials (BAPs), normalized per neuron, binned in 50 μm increments from the soma ($F(245) = 33.28$, $p = 2.4*10^{-8}$, ANOVA).

(B) The number of BAPs, normalized per neuron, averaged separately for each neuron's apical branch and basal branches ($F(303) = 34.88$, $p = 9.4*10^{-9}$, ANOVA).

(C) The number of BAPs, normalized per neuron, binned in 50 μm increments from the soma for apical dendrites and 20 μm increments for basal dendrites (apical only: $F(151) = 6.7$, $p = 0.01$. Basal only: $F(92) = 7.61$, $p = 7.0*10^{-3}$, ANOVA).

(D) Graphical representation of BAP attenuation with increasing distance from the soma.

(E) Responsive spine tuning correlation to the soma averaged for each responsive and unresponsive neuron (bar plots, $t(20) = 2.93$, $p = 8.3*10^{-3}$, two-sample *t* test) and of all responsive spines on responsive and unresponsive neurons (boxplots, $F(656) = 9.32$, $p = 2.4*10^{-3}$, ANOVA).

(F) The mean somatic tuning correlation of responsive spines on apical and basal branches of responsive neurons.

(G) Spine-to-soma correlation of spines on responsive neurons binned in 50 μm increments from the soma ($F(280) = 5.00$, $p = 0.026$, ANOVA).

(H) Partial correlation for responsive neurons between a spine's tuning correlation to the soma and its distance from the soma, controlling for the effect of branch type ($t(6) = -3.76$, $p = 9.4*10^{-3}$, one-sample *t* test). For bar plots, circles or lines show the mean(s) of each neuron, while the bars show the mean of each group. Boxplots show the median (red line), 25$^{th}$ and 75$^{th}$ percentiles (box edges), the most extreme non-outlier values (lines), and outliers (crosses). Error bars show the standard error of each group or bin. * denotes a significant effect or difference.

branch type, or distance from the soma predict the fraction of spines overall that are responsive in each segment of the dendrite? As expected, responsive neurons had more visually responsive spines than did unresponsive neurons (Figure 3A). When categorized by branch type, the fraction of apical responsive spines remained significantly higher on responsive neurons than on unresponsive neurons, but the fraction of basal responsive spines was not significantly different (Figure 3B). Interestingly, on unresponsive neurons, apical branches had significantly fewer responsive spines than did basal branches. Distance from the soma, on the other hand, was not significantly correlated with the fraction of responsive spines (Figures 3C and 3D). Thus, proportionally fewer responsive spines were found in the apical compartment of unresponsive neurons, resulting in fewer responsive spines overall compared to responsive neurons.

Despite these differences in the fraction of responsive spines, the quality of visual input as measured by orientation selectivity (OSI), direction selectivity (DSI), and reliability (Figure S2A) was comparable between responsive and unresponsive neurons (Figures S2B–S2D) and across branch types (Figures S2E–S2G). There was a significant negative partial correlation of distance from the soma on OSI and DSI when controlling for branch type, but only for unresponsive neurons (Figures S2H–S2J). Thus, we conclude that somatic responsiveness and branch type correlate with the fraction of visually responsive spines; however, we observed no significant differences in the quality of that input.

## Tuning correlation between spine pairs on responsive neurons varies significantly with inter-spine distance

We next examined how spines were organized relative to one another based on the similarity of their visual tuning (signal/tuning correlation).[31] We hypothesized that spines on responsive neurons would have higher mean tuning correlations because of their shared bias toward the parent soma's preferred stimulus (Figures 1H and 2E). Indeed, the mean pairwise tuning correlation between responsive spines on responsive neurons was significantly higher than on unresponsive neurons (Figure 4A). There was no difference in mean pairwise tuning correlation between spines on apical or basal branches (Figure 4B), and we found no significant effect of distance from the soma on the tuning correlation between pairs of spines (Figures 4C and 4D). We observed the same effects when measuring tuning similarity using orientation dispersion rather than tuning correlation (Figures S3A–S3C and S4).[32] Thus, pairwise spine correlation

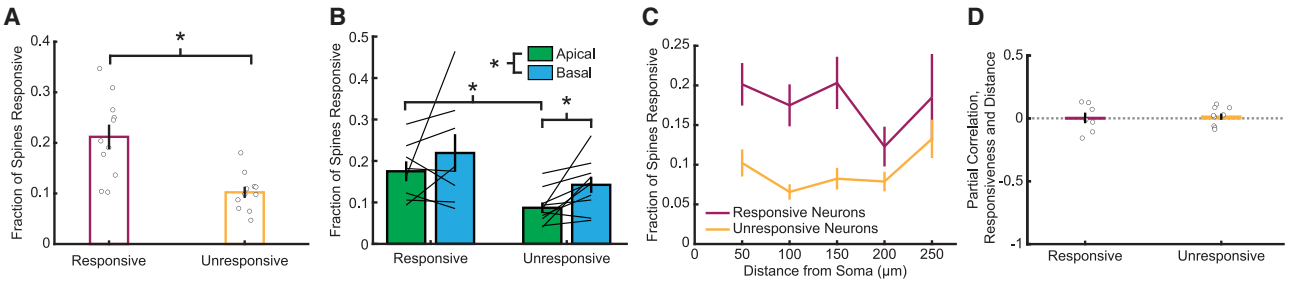



**Figure 3. Neurons with visually responsive somata have more visually responsive spines**

(A) The fraction of responsive spines on responsive and unresponsive neurons ($t(20) = 4.13$, $p = 5.2*10^{-4}$, two-sample $t$ test).

(B) The fraction of responsive spines on the apical and basal branches of responsive and unresponsive neurons (responsive vs. unresponsive apical: $t(16) = 3.4$, $p = 3.5*10^{-3}$; basal: $t(16) = 1.7$, $p = 0.11$, two-sample $t$ test. Responsive neuron apical vs. basal: $t(7) = -1.1$, $p = 0.32$; unresponsive neuron apical vs. basal: $t(9) = -3.0$, $p = 0.014$, paired $t$ test. Overall apical vs. basal: $t(17) = -2.5$, $p = 0.023$, paired $t$ test).

(C) Fraction of responsive spines on dendritic segments from responsive and unresponsive neurons, binned in 50 μm increments from the soma.

(D) Partial correlation for each neuron between spine responsiveness and distance from the soma, controlling for the effect of branch type (Responsive: $t(6) = 0.09$, $p = 0.93$. Unresponsive $t(8) = 0.57$, $p = 0.59$, one-sample $t$ test). For bar plots, circles or lines show the mean(s) of each neuron, while the bars show the mean of each group. Error bars show the standard error of each group or bin. * denotes a significant difference between groups.

is higher globally on visually responsive neurons, while no significant differences were observed between apical and basal branches or with distance from the soma.

We next examined the organization of spines locally within a dendritic segment (Figure 4E), as spines with similar functional properties or activity are known to cluster together on pyramidal neuron branches in different brain regions.[13,33–36] We first asked whether responsive spines were located closer to other responsive spines than would be expected by chance. For responsive and unresponsive neurons, we measured the median pairwise distance between responsive spines only and compared this to a distribution of median distances computed after repeatedly shuffling all spine pairwise distances within each segment (randomization test, see STAR Methods). While the distance between responsive spine pairs was not significantly different between responsive and unresponsive neurons (Figure S3D), responsive spine pairs were closer together than expected by chance on responsive neurons (Figure S3E).

We then examined whether spine pairs clustered based on shared tuning correlation by binning responsive spine pairs by their inter-spine distance in 5 μm increments and comparing the mean pairwise tuning correlation in each bin to a distribution generated using their shuffled distances, as has been done previously[26–28,34] with significance computed from comparing the real data in each bin to the shuffled data (randomization test, see STAR Methods). We found that responsive spine pairs on responsive neurons that were <5 μm apart had significantly higher tuning correlations than expected by chance (Figure 4F), and spine pairs ≥5 μm but <10 μm apart were significantly less correlated than chance. No significant effect of spine pair distance on tuning correlation was detected for unresponsive neurons. For the responsive neurons only, we separately examined spine pairs on apical versus basal branches and at proximal versus distal locations to determine if clustering differed by branch type and/or distance from the soma, respectively. The degree of clustering within each 5 μm bin was not significantly different between apical and basal spine pairs (Figure S3F) or proximal and distal spine pairs (Figure S3G). We conclude that synaptic inputs to responsive neurons are organized locally: Pairwise tuning correlation is higher than chance for spines located <5 μm apart but lower for spines located ≥5 μm but <10 μm apart, reflecting a possible distance-dependent biphasic organization of synaptic inputs on dendrites.[3]

## Somatically correlated inputs are more selective and closer to the soma

There are many factors, in addition to distance, that likely account for the variance in a spine's correlation to its soma (Figure 5A). For example, increased spine-to-soma correlation may indicate a functional link between that input and somatic output, consistent with the spine's reliability or size.[37] Reciprocally, spike-timing-dependent plasticity rules suggest that spines correlated to the soma should be preferentially retained or strengthened while uncorrelated spines are removed or weakened.[5,8,10,38] Due to the number of predictors and possible correlations between them, we used mixed-effects linear modeling and 5-fold cross-validation to isolate their effects. In models containing a single predictor, OSI and distance from the soma were significant predictors of spine-to-soma correlation (Figure 5B). We then trained a full model with all predictors and models with one predictor left out for each fold/repetition's training data and computed the $R^2$ for the test data. The difference in $R^2$ from the full model for each "leave-one-out" model gives the putative variance explained by each left-out predictor for each fold/repetition. We compared the distribution of mean variance explained across repetitions of 5-fold cross-validation via a one-sided bootstrap test (variance explained >0), corrected for multiple comparisons. From this analysis, we found that OSI, DSI, size, and distance from the soma each account for unique portions of the total explained variance in spine-to-soma correlation, with OSI explaining the most variance (Figure 5C).

We next wondered if we could predict the mean spine-to-soma correlation for each responsive neuron using the soma's response properties, namely the somatic OSI, DSI, and reliability. Neither somatic OSI (Figure 5D) nor DSI (Figure 5E)

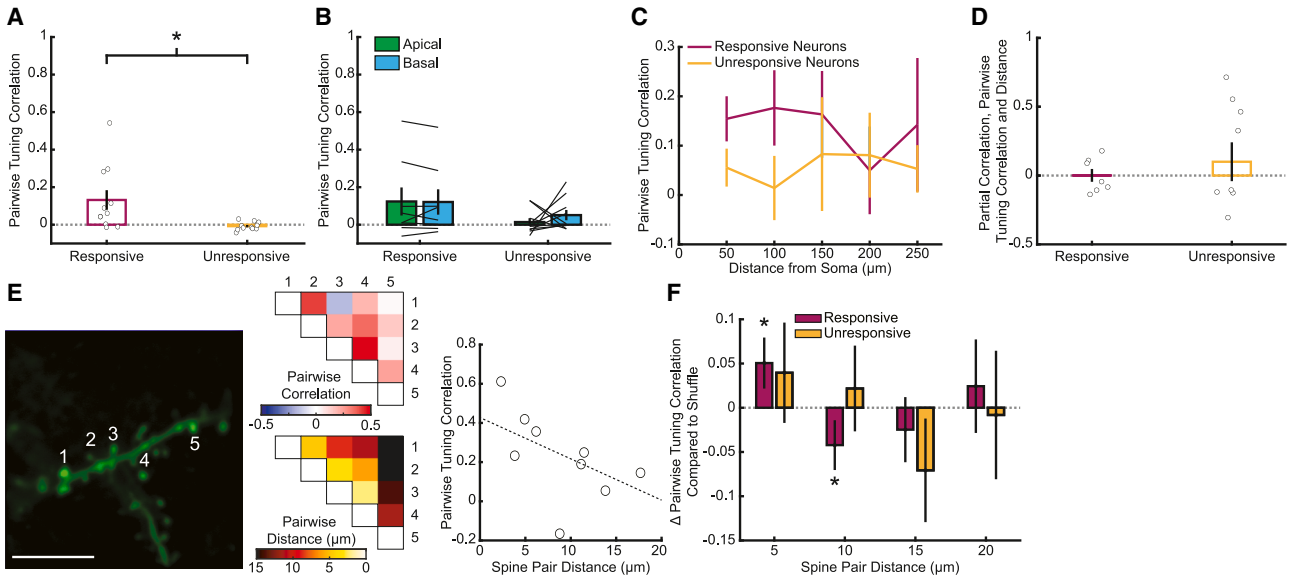



**Figure 4. Tuning correlation between spine pairs on responsive neurons varies significantly with inter-spine distance**

(A) Mean pairwise tuning correlation between all responsive spines on responsive and unresponsive neurons ($t(20) = 2.65$, $p = 0.015$, two-sample $t$ test).

(B) Mean pairwise tuning correlation between all responsive spines on each neuron's apical and basal branches (responsive: $t(7) = 0.18$, $p = 0.86$. Unresponsive: $t(9) = -0.89$, $p = 0.40$, paired $t$ test).

(C) Mean pairwise correlation between responsive spines on dendritic segments from responsive and unresponsive neurons, binned in 50 μm increments from the soma (responsive: $F(66) = 0.87$, $p = 0.35$; unresponsive: $F(62) = 0.06$, $p = 0.81$).

(D) Partial correlation between spine pair tuning correlation and distance from soma controlling for the effect of branch type. Only spine pairs within the same imaged segment were used (responsive: $t(6) = 0.05$, $p = 0.96$; unresponsive: $t(8) = 0.46$, $p = 0.66$, one-sample $t$ test).

(E) An example dendritic segment with responsive spines indicated by white numbers (left. Scale bars, 10 μm). Heatmaps of pairwise tuning correlation and distance between the spine pairs of the example dendritic segment (middle). Scatterplot of the pairwise tuning correlation and distance between the spine pairs of the example dendritic segment (right).

(F) Tuning correlation between dendritic spine pairs as a function of their distance apart, binned in 5 μm increments, for responsive and unresponsive neurons (664 pairs on responsive neurons, 135 pairs on unresponsive neurons. Responsive: < 5 μm, $p < 1*10^{-4}$. ≥5 μm to <10 μm, $p = 0.04$, randomization test). For bar plots, circles or lines show the mean(s) of each neuron, while the bars show the mean of each group. Error bars show the standard error of each group or bin. * denotes a significant difference between groups or a significant difference from the shuffle for a bin.

showed a statistically significant relationship with mean spine-to-soma correlation. However, somatic reliability was positively correlated to mean spine-to-soma correlation (Figure 5F). In summary, we found that orientation-selective spines near the soma had higher tuning correlation to the soma, and that neurons with higher mean spine-to-soma correlation had more reliable responses to their preferred stimulus.

Our results reveal that synaptic inputs to excitatory layer 2/3 neurons in mouse V1 are not randomly arranged but organized and distributed in a manner that correlates with multiple factors, including somatic responsiveness, somatic tuning, branch type, distance from the soma, local correlations, and stimulus selectivity.

## DISCUSSION

We examined the functional properties and organization of synaptic inputs on layer 2/3 excitatory neurons in mouse V1, asking whether their properties correlate with their position within the dendritic arbor, location on an apical or basal branch, distance from the soma, distance from other spines, and the visually tuned somatic feedback they receive. We explored this organization for each neuron, recording the response of its soma and multiple dendritic spines to the same set of stimuli. We first confirmed that the reliability of BAP transmission, as measured through calcium activity, decreases as a function of the distance from the soma in both apical and basal dendrites. Responsive spines proximal to the soma were more correlated to the soma than distal spines. The fraction of responsive spines was higher on basal branches than on apical branches, but responsive neurons had more responsive spines on their apical branch than did unresponsive neurons. Responsive neurons had higher global pairwise tuning correlation between their dendritic spines than did unresponsive neurons, and spines were locally clustered in a distance-dependent biphasic manner, with spines <5 μm apart showing higher correlations and those ≥5 but <10 μm apart showing lower correlations than expected by chance. Neither the global nor local pairwise organization of spines showed significant variation based on branch type or distance from the soma. Finally, spines with higher orientation selectivity close to the soma had higher tuning correlation to the soma, and neurons with higher mean spine-to-soma correlation had more reliable responses to their preferred stimulus. In summary, rather than being randomly distributed, synaptic visual input to dendritic spines of V1 layer 2/3

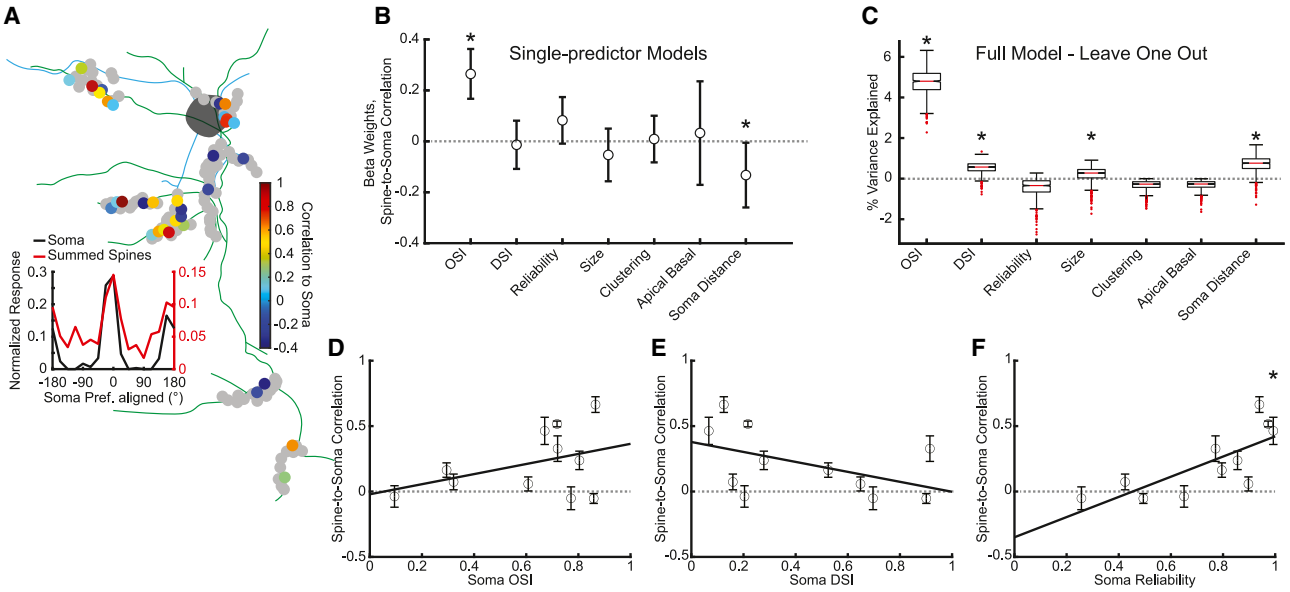



**Figure 5. Somatically correlated inputs are more selective and closer to the soma**

(A) Diagram of a visually responsive neuron with apical (green) and basal (blue) branches. Imaged spines are represented by circles on the dendrites, with unresponsive spines colored gray and responsive spines colored by their tuning correlation to the soma. The red tuning curve represents the linear sum of the median trial response to each direction for all responsive spines, aligned to the preferred direction of the soma (black) and normalized to the sum of responses to all directions (inset).

(B) Median weights and lower/upper bounds for each predictor used in multiple permutations of a single predictor linear mixed effects model (OSI: $t(296) = 5.33$, $p = 2.0*10^{-7}$; distance from the soma ($t(225) = -2.06$, $p = 0.041$. Medians from 1,000 rounds of 5-fold cross-validation).

(C) Boxplot of variance in spine-to-soma tuning correlation explained by each predictor, calculated from multiple permutations of comparing a linear mixed effects model with all predictors to a model trained on the same subset of data but missing one predictor (OSI: $p < 10^{-4}$; DSI: $p < 10^{-4}$; spine size: $p < 10^{-4}$; distance from soma: $p < 10^{-4}$. bootstrap permutation test ($p$ less than measurable given number of bootstraps)).

(D) Correlation between somatic OSI and the mean spine-to-soma tuning correlation of each responsive neuron (rho(9) = 0.40, $p = 0.67$ corrected for multiple comparisons).

(E) Same as in D., but for somatic DSI (rho(9) = −0.48, $p = 0.40$ corrected for multiple comparisons).

(F) Same as in D., but for somatic reliability to each neurons' preferred stimulus (rho(9) = 0.76, $p = 0.021$ corrected for multiple comparisons). Error bars in panel B show the 95% confidence intervals. Boxplots show the median (red line), 25$^{th}$ and 75$^{th}$ percentiles (box edges), the most extreme non-outlier values (lines), and outliers (crosses). Line plots show the trend line between the two variables, with each neuron represented by a dot, with the error bars showing the standard error of spine-to-soma correlation within that neuron. * denotes a significant predictor or correlation.

pyramidal neurons exhibits organization that corresponds to its correlation to the soma, correlation to its neighbors, distance from the soma, selectivity, and branch type.

One hypothesis to explain the differences between spines on responsive and unresponsive neurons would be that spines on responsive neurons receive visually tuned feedback in the form of BAPs while spines on unresponsive neurons do not. Alternatively, it is equally plausible that these synaptic differences are what make a neuron more or less likely to be visually responsive in the first place. It is probable that our findings are a mixture of these two possibilities, in which a subset of synaptic differences accounts for the initial somatic responsiveness and another subset emerges in alignment with the subsequent somatic feedback stabilizing or refining spine responses.[5] In mice, orientation-selective responses emerge even when spontaneous and evoked firing are suppressed during development.[39] A similar approach could be used to address whether spines on these suppressed neurons develop organization like that which we observe, suggesting that the organization is independent of somatic activity, or if the organization emerges only after somatic activity is restored.

The somatically correlated presynaptic inputs may arise from local neurons within V1, as similarly tuned layer 2/3 V1 neurons are known to be preferentially, and recurrently, connected.[7,8,38] The spines that are more correlated to the soma, then, are likely to reflect input from similarly tuned, neighboring cortical neurons.[40] This may account for why, in our data, a spine's OSI was the most significant predictor of correlation to the soma, as V1 neurons are more orientation-selective than inputs from the lateral geniculate nucleus of the thalamus.[41,42] Indeed, on layer 2/3 pyramidal neurons in V1, only 5.8% of spines receive thalamic input.[43] Like-to-like connectivity in layer 2/3 is predicted to arise from mechanisms of spike-timing-dependent plasticity.[10] The decrease in spine-to-soma correlation we observed with increasing distance from the soma aligns to this prediction, as NMDA-receptor-dependent long-term potentiation driven by pre-post action potential pairing decreases with increasing distance from the soma.[44] Attenuation of BAPs propagating from the soma could lead to lower or less reliable levels

**Table 1. Biological and technical variables of each subject**

| Mouse ID | Cell ID | Sex | DOB | Imaging Start | Age (days) | Days Imaged | Degree Increment | Spatial Frequency | Depth (μm) | Soma responsive | Fields of View | Reconstructed | Unique Basal Branches | Spines | Resp. Spines |
|---|---|---|---|---|---|---|---|---|---|---|---|---|---|---|---|
| ASC10 | 2 | Female | 2020-07-18 | 2020-09-09 | 53 | 8 | 22.5 | 0.02 | 81 | No | 19 | Yes | 2 | 331 | 47 |
| ASC11 | 4 | Female | 2020-07-24 | 2020-09-13 | 51 | 4 | 22.5 | 0.02 | 120 | No | 7 | Yes | 1 | 143 | 14 |
| ASC12 | 1 | Female | 2020-07-24 | 2020-09-13 | 51 | 5 | 22.5 | 0.02 | 111 | No | 11 | Yes | 2 | 183 | 33 |
| ASC15 | 1 | Male | 2020-08-30 | 2020-10-16 | 47 | 7 | 22.5 | 0.02 | 151 | No | 23 | No | – | 339 | 37 |
| ASC16 | 1 | Male | 2020-08-30 | 2020-10-17 | 48 | 7 | 22.5 | 0.02 | 142 | Yes | 20 | Yes | 1 | 336 | 35 |
| ASC17 | 2 | Female | 2020-09-10 | 2020-11-07 | 58 | 11 | 22.5 | 0.02 | 153 | No | 16 | Yes | 2 | 263 | 23 |
| ASC17 | 3 | Female | 2020-09-10 | 2020-11-10 | 61 | 6 | 22.5 | 0.02 | 174 | No | 22 | Yes | 2 | 340 | 16 |
| ASC18 | 2 | Female | 2020-09-10 | 2020-11-07 | 58 | 13 | 22.5 | 0.02 | 111 | No | 39 | Yes | 2 | 708 | 50 |
| ASC18 | 3 | Female | 2020-09-10 | 2020-11-25 | 76 | 4 | 22.5 | 0.02 | 206 | No | 12 | Yes | 2 | 254 | 25 |
| ASC20 | 3 | Male | 2020-11-24 | 2021-01-20 | 57 | 5 | 22.5 | 0.02 | 169 | Yes | 17 | Yes | 2 | 231 | 44 |
| ASC22 | 2 | Female | 2021-03-03 | 2021-04-21 | 49 | 8 | 22.5 | 0.04 | 122 | Yes | 17 | Yes | 2 | 263 | 27 |
| ASC23 | 2 | Female | 2021-03-03 | 2021-04-21 | 49 | 9 | 22.5 | 0.04 | 190 | No | 18 | Yes | 2 | 231 | 15 |
| ASC24 | 2 | Male | 2021-04-25 | 2021-06-21 | 57 | 8 | 22.5 | 0.04 | 107 | Yes | 23 | Yes | 2 | 382 | 118 |
| ASC26 | 3 | Female | 2022-02-14 | 2022-05-14 | 89 | 3 | 22.5 | 0.04 | 236 | Yes | 11 | Yes | 2 | 136 | 34 |
| ASC26 | 4 | Female | 2022-02-14 | 2022-05-16 | 91 | 2 | 22.5 | 0.04 | 141 | No | 7 | Yes | 2 | 88 | 10 |
| ASC27 | 1 | Male | 2022-02-14 | 2022-05-14 | 89 | 7 | 22.5 | 0.04 | 128 | Yes | 16 | Yes | 2 | 198 | 27 |
| ASC28 | 3 | Male | 2022-02-14 | 2022-05-22 | 97 | 7 | 22.5 | 0.04 | 179 | Yes | 8 | Yes | 3 | 62 | 11 |
| BM016 | 4 | Male | 2022-07-10 | 2022-08-12 | 33 | 1 | 45 | 0.02 | 135 | Yes | 4 | No | – | 102 | 25 |
| BM018 | 4 | Female | 2022-07-23 | 2022-08-25 | 33 | 1 | 45 | 0.02 | 190 | Yes | 3 | No | 0 | 49 | 13 |
| BM020 | 3 | Female | 2022-08-20 | 2022-09-22 | 33 | 1 | 45 | 0.08 | 161 | No | 4 | No | – | 142 | 16 |
| BM026 | 2 | Female | 2022-12-31 | 2023-02-03 | 34 | 1 | 45 | 0.02 | 121 | Yes | 5 | No | 0 | 103 | 21 |
| BM029 | 12 | Male | 2023-02-11 | 2023-03-17 | 34 | 1 | 45 | 0.04 | 153 | Yes | 3 | No | 0 | 49 | 17 |

of NMDA receptor activation during the tight temporal window required for classical spike timing dependent plasticity. However, it should be noted that in our results the gradual attenuation of BAPs is contrasted by the sharper falloff in spine-to-soma correlation. This could indicate that BAP attenuation and decreasing spine-to-soma correlation are unrelated or that spike-timing-dependent long-term potentiation depends on additional factors, such as the activation of voltage-sensitive channels, not measured here.

This like-to-like plasticity should also be reflected in an increased size of correlated spines through structural potentiation, and indeed synapses between neurons with similar tuning are, on average, larger than those between neurons with dissimilar tuning, and spine size correlates to synaptic strength *in vivo*.[8,37,38] Contrary to this, large spines on layer 2/3 neurons in ferret V1 were not found to be significantly more correlated to the soma than small spines.[28] Similarly, in our data from mouse layer 2/3 neurons, we found no detectable positive association between spine size and spine-to-soma correlation. As our results are purely correlational, we cannot conclude if spine-to-soma correlation arises as a consequence of spike-timing-dependent plasticity through BAPs or if, instead, somatic responsiveness simply requires some coincident threshold of visual input with shared tuning, as previously suggested.[28]

Our results show that responsive neurons have a higher fraction of responsive spines on their apical dendrite than unresponsive neurons do. This may indicate that somatic visual responsiveness is linked to a specific threshold of visually tuned input on the apical dendrite. Supporting a potential role for the apical dendrite in shaping neuronal responsiveness, apical morphology, and apical input asymmetry of layer 2/3 neurons in mouse V1 correlate with neuronal orientation and direction selectivity, respectively.[24] However, ablation of the apical branch has been shown not to alter orientation tuning,[45] which would suggest that the main synaptic drive originates from basal dendrites. Paired somatic and spine recordings, potentially with selective silencing of apical or basal dendrites, could help to address this discrepancy.

Functional clustering of spines based on spontaneous activity[13] and receptive field location[26] has been previously observed in layer 2/3 neurons of mouse V1. Unlike in ferret or macaque V1,[32,46] spines on mouse V1 neurons with similar orientation preference were initially not found to cluster together above chance levels,[6,26] with the exception of clustering between callosal and non-callosal spine pairs.[27] In contrast, a more recent study observed clustering of spines with similar orientation preference, albeit with a small sample size, similar to the clustering we observed.[47] Namely, we observed a distance-dependent biphasic organization of spines with nearby-higher distant-lower organization based on the correlation of their tuning. A similar organization has been hypothesized to be driven by heterosynaptic plasticity in mouse V1 dendrites,[3] where co-active neighboring spines are strengthened by the spread of calcium and other signaling molecules.[12,48] At intermediate distances, other spines are then de-potentiated or weakened to compensate. At further distances, the effects of heterosynaptic plasticity dissipate, and correlations return to baseline levels for that neuron. Clustering is thought to require neuronal activity and NMDA receptor activation,[49–52] which could explain why significant clustering was detected on only responsive neurons.

In conclusion, our findings reveal that the dendritic arbor of layer 2/3 neurons is not merely a passive recipient of diverse inputs but is structured by spatial and functional logic. Our results underscore the idea that synaptic distribution reflects an underlying organizational principle that aligns individual synaptic properties with the output of the whole cell. By demonstrating that synaptic organization correlates with somatic and local feedback, this work provides a framework for understanding how the physical architecture of a neuron facilitates the integration of sensory information. Elucidating these patterns is a critical step toward deciphering the rules that allow individual neurons to transform heterogeneous synaptic signals into coherent sensory representations.

## Limitations of the study

While our findings reveal several synaptic organizational principles of layer 2/3 V1 neurons, there are multiple limitations to consider. First and most importantly, our results are purely correlational. Although we demonstrate that factors such as dendritic distance, branch type, and somatic responsiveness vary alongside spine properties such as spine-to-soma correlation, we cannot conclude the cause of the observed organization. For instance, while backpropagating action potentials and spine-to-soma correlation both decrease with distance from the soma, we have not experimentally manipulated backpropagating action potentials to prove their instructive role through spine plasticity. Second, it should be kept in mind that most *in vivo* studies of synaptic input, including ours, rely on imaging postsynaptic calcium dynamics in spines. While two-photon calcium imaging of spines is a powerful tool for mapping functional inputs, synaptic calcium signals are contaminated by dendritic calcium events, which must be computationally removed[2,26,27] with varying success,[35] and are largely NMDA receptor driven,[53] thus missing smaller AMPA-receptor-driven sodium currents. Recent studies utilizing newly developed fluorescent glutamate indicators *in vivo* are helping to address these limitations,[46,47] and when paired with a red-shifted calcium indicator, allow for all-optical, *in vivo*, simultaneous measurements of synaptic input and somatic output.[11,47] Third, our study focuses on excitatory synaptic inputs only. Inhibition is a critical component in shaping a variety of visual responses[54,55] and the number of inhibitory synapses is known to vary with distance from the soma.[56] It is possible that these inhibitory synapses are also organized functionally based on their correlated activity with each other and with the soma, but this has yet to be explored. Future studies mapping both excitatory and inhibitory input to single neurons will provide a much clearer picture of how these opposing forces interact, and how these interactions vary as a function of dendritic properties.

## RESOURCE AVAILABILITY

### Lead contact

Requests for further information and resources should be directed to and will be fulfilled by the lead contact, Mriganka Sur (msur@mit.edu).

### Materials availability

This study did not generate new unique reagents.

### Data and code availability

- Pre-processed imaging data have been deposited as .mat files and are publicly available at Zenodo: https://doi.org/10.5281/zenodo.19372968.
- Raw imaging data reported in this paper will be shared by the lead contact upon request.
- All code has been deposited and is publicly available at Zenodo: https://doi.org/10.5281/zenodo.18552067.
- Any additional information required to reanalyze the data reported in this paper is available from the lead contact upon request.

## ACKNOWLEDGMENTS

This work was supported by NIH grants R01MH085802 (M.S.), R01MH126351 (M.S.), F32EY032756 (K.J.), and F31EY033649 (K.T.). This work was additionally supported by the Simons Foundation Autism Research Initiative through the Simons Center for the Social Brain, MIT (M.S.). We thank Taylor Johns, Marco Celotto, and other members of the Sur lab for their advice, help, and support.

## AUTHOR CONTRIBUTIONS

K.J., K.T., J.I., and M.S. conceived the experimental design with input from others. K.J. and K.T. performed all surgeries and recordings. K.J., K.T., and A.R. analyzed all the two-photon imaging data. G.H. and K.M. performed structural analysis. K.J. and M.S. wrote the manuscript with input from others. All authors edited the manuscript and read and approved the final version.

## DECLARATION OF INTERESTS

The authors declare no competing financial interests.

## DECLARATION OF GENERATIVE AI AND AI-ASSISTED TECHNOLOGIES IN THE WRITING PROCESS

During the preparation of this work, the authors used Google Gemini to proofread sections of the text for grammar and clarity. After using this tool, the authors reviewed and edited the content as needed and take full responsibility for the content of the published article.

## STAR★METHODS

Detailed methods are provided in the online version of this paper and include the following:

- KEY RESOURCES TABLE
- EXPERIMENTAL MODEL AND STUDY PARTICIPANT DETAILS
- METHOD DETAILS
  - Surgical preparation
  - Two-photon imaging
  - Image processing and ROI selection
  - Functional analysis for two-photon imaging data
  - Structural analysis of two-photon imaging data
- QUANTIFICATION AND STATISTICAL ANALYSIS

## SUPPLEMENTAL INFORMATION

Supplemental information can be found online at https://doi.org/10.1016/j.isci.2026.115861.

Received: December 19, 2025
Revised: February 10, 2026
Accepted: April 20, 2026
Published: April 22, 2026

## REFERENCES

1. Niell, C.M., and Scanziani, M. (2021). How Cortical Circuits Implement Cortical Computations: Mouse Visual Cortex as a Model. Annu. Rev. Neurosci. *44*, 517–546. https://doi.org/10.1146/annurev-neuro-102320-085825.
2. Chen, T.-W., Wardill, T.J., Sun, Y., Pulver, S.R., Renninger, S.L., Baohan, A., Schreiter, E.R., Kerr, R.A., Orger, M.B., Jayaraman, V., et al. (2013). Ultrasensitive fluorescent proteins for imaging neuronal activity. Nature *499*, 295–300. https://doi.org/10.1038/nature12354.
3. El-Boustani, S., Ip, J.P.K., Breton-Provencher, V., Knott, G.W., Okuno, H., Bito, H., and Sur, M. (2018). Locally coordinated synaptic plasticity of visual cortex neurons in vivo. Science *360*, 1349–1354. https://doi.org/10.1126/science.aao0862.
4. Kirchner, J.H., and Gjorgjieva, J. (2021). Emergence of local and global synaptic organization on cortical dendrites. Nat. Commun. *12*, 4005. https://doi.org/10.1038/s41467-021-23557-3.
5. Tsimring, K., Jenks, K.R., Cusseddu, C., Heller, G.R., Ip, J.P.K., Gjorgjieva, J., and Sur, M. (2025). Large-scale synaptic dynamics drive the reconstruction of binocular circuits in mouse visual cortex. Nat. Commun. *16*, 5810. https://doi.org/10.1038/s41467-025-60825-y.
6. Jia, H., Rochefort, N.L., Chen, X., and Konnerth, A. (2010). Dendritic organization of sensory input to cortical neurons in vivo. Nature *464*, 1307–1312. https://doi.org/10.1038/nature08947.
7. Ko, H., Hofer, S.B., Pichler, B., Buchanan, K.A., Sjöström, P.J., and Mrsic-Flogel, T.D. (2011). Functional specificity of local synaptic connections in neocortical networks. Nature *473*, 87–91. https://doi.org/10.1038/nature09880.
8. Cossell, L., Iacaruso, M.F., Muir, D.R., Houlton, R., Sader, E.N., Ko, H., Hofer, S.B., and Mrsic-Flogel, T.D. (2015). Functional organization of excitatory synaptic strength in primary visual cortex. Nature *518*, 399–403. https://doi.org/10.1038/nature14182.
9. Ding, Z., Fahey, P.G., Papadopoulos, S., Wang, E.Y., Celii, B., Papadopoulos, C., Chang, A., Kunin, A.B., Tran, D., Fu, J., et al. (2025). Functional connectomics reveals general wiring rule in mouse visual cortex. Nature *640*, 459–469. https://doi.org/10.1038/s41586-025-08840-3.
10. Ko, H., Cossell, L., Baragli, C., Antolik, J., Clopath, C., Hofer, S.B., and Mrsic-Flogel, T.D. (2013). The emergence of functional microcircuits in visual cortex. Nature *496*, 96–100. https://doi.org/10.1038/nature12015.
11. Wright, W.J., Hedrick, N.G., and Komiyama, T. (2025). Distinct synaptic plasticity rules operate across dendritic compartments in vivo during learning. Science *388*, 322–328. https://doi.org/10.1126/science.ads4706.
12. Jenks, K.R., Tsimring, K., Ip, J.P.K., Zepeda, J.C., and Sur, M. (2021). Heterosynaptic Plasticity and the Experience-Dependent Refinement of Developing Neuronal Circuits. Front. Neural Circuits *15*, 803401. https://doi.org/10.3389/fncir.2021.803401.
13. Leighton, A.H., Cheyne, J.E., and Lohmann, C. (2024). Clustered synapses develop in distinct dendritic domains in visual cortex before eye opening. eLife *12*, RP93498. https://doi.org/10.7554/eLife.93498.
14. Segev, I., Häusser, M., Rinzel, J., and Shepherd, G.M. (2018). Wilfrid Rall (1922–2018). Neuron *99*, 877–879.
15. Larkum, M.E., Zhu, J.J., and Sakmann, B. (2001). Dendritic mechanisms underlying the coupling of the dendritic with the axonal action potential initiation zone of adult rat layer 5 pyramidal neurons. J. Physiol. *533*, 447–466. https://doi.org/10.1111/j.1469-7793.2001.0447a.x.
16. Waters, J., Larkum, M., Sakmann, B., and Helmchen, F. (2003). Supralinear $Ca^{2+}$ Influx into Dendritic Tufts of Layer 2/3 Neocortical Pyramidal Neurons *In Vitro* and *In Vivo*. J. Neurosci. *23*, 8558–8567. https://doi.org/10.1523/JNEUROSCI.23-24-08558.2003.
17. Nevian, T., Larkum, M.E., Polsky, A., and Schiller, J. (2007). Properties of basal dendrites of layer 5 pyramidal neurons: a direct patch-clamp recording study. Nat. Neurosci. *10*, 206–214. https://doi.org/10.1038/nn1826.

18. Cho, K.-H., Jang, H.J., Lee, E.H., Yoon, S.H., Hahn, S.J., Jo, Y.H., Kim, M.S., and Rhie, D.J. (2008). Differential Cholinergic Modulation of $Ca^{2+}$ Transients Evoked by Backpropagating Action Potentials in Apical and Basal Dendrites of Cortical Pyramidal Neurons. J. Neurophysiol. *99*, 2833–2843. https://doi.org/10.1152/jn.00063.2008.

19. Hill, D.N., Varga, Z., Jia, H., Sakmann, B., and Konnerth, A. (2013). Multibranch activity in basal and tuft dendrites during firing of layer 5 cortical neurons in vivo. Proc. Natl. Acad. Sci. USA *110*, 13618–13623. https://doi.org/10.1073/pnas.1312599110.

20. Palmer, L.M., Shai, A.S., Reeve, J.E., Anderson, H.L., Paulsen, O., and Larkum, M.E. (2014). NMDA spikes enhance action potential generation during sensory input. Nat. Neurosci. *17*, 383–390. https://doi.org/10.1038/nn.3646.

21. Petreanu, L., Mao, T., Sternson, S.M., and Svoboda, K. (2009). The subcellular organization of neocortical excitatory connections. Nature *457*, 1142–1145. https://doi.org/10.1038/nature07709.

22. Rees, C.L., Moradi, K., and Ascoli, G.A. (2017). Weighing the Evidence in Peters' Rule: Does Neuronal Morphology Predict Connectivity? Trends Neurosci. *40*, 63–71. https://doi.org/10.1016/j.tins.2016.11.007.

23. Lafourcade, M., van der Goes, M.S.H., Vardalaki, D., Brown, N.J., Voigts, J., Yun, D.H., Kim, M.E., Ku, T., and Harnett, M.T. (2022). Differential dendritic integration of long-range inputs in association cortex via subcellular changes in synaptic AMPA-to-NMDA receptor ratio. Neuron *110*, 1532–1546.e4. https://doi.org/10.1016/j.neuron.2022.01.025.

24. Weiler, S., Guggiana Nilo, D., Bonhoeffer, T., Hübener, M., Rose, T., and Scheuss, V. (2022). Orientation and direction tuning align with dendritic morphology and spatial connectivity in mouse visual cortex. Curr. Biol. *32*, 1743–1753.e7. https://doi.org/10.1016/j.cub.2022.02.048.

25. Montijn, J.S., Seignette, K., Howlett, M.H., Cazemier, J.L., Kamermans, M., Levelt, C.N., and Heimel, J.A. (2021). A parameter-free statistical test for neuronal responsiveness. eLife *10*, e71969. https://doi.org/10.7554/eLife.71969.

26. Iacaruso, M.F., Gasler, I.T., and Hofer, S.B. (2017). Synaptic organization of visual space in primary visual cortex. Nature *547*, 449–452. https://doi.org/10.1038/nature23019.

27. Lee, K.-S., Vandemark, K., Mezey, D., Shultz, N., and Fitzpatrick, D. (2019). Functional Synaptic Architecture of Callosal Inputs in Mouse Primary Visual Cortex. Neuron *101*, 421–428.e5. https://doi.org/10.1016/j.neuron.2018.12.005.

28. Scholl, B., Thomas, C.I., Ryan, M.A., Kamasawa, N., and Fitzpatrick, D. (2021). Cortical response selectivity derives from strength in numbers of synapses. Nature *590*, 111–114. https://doi.org/10.1038/s41586-020-03044-3.

29. Antic, S.D. (2003). Action Potentials in Basal and Oblique Dendrites of Rat Neocortical Pyramidal Neurons. J. Physiol. *550*, 35–50. https://doi.org/10.1113/jphysiol.2002.033746.

30. Kampa, B.M., and Stuart, G.J. (2006). Calcium Spikes in Basal Dendrites of Layer 5 Pyramidal Neurons during Action Potential Bursts. J. Neurosci. *26*, 7424–7432. https://doi.org/10.1523/JNEUROSCI.3062-05.2006.

31. Averbeck, B.B., Latham, P.E., and Pouget, A. (2006). Neural correlations, population coding and computation. Nat. Rev. Neurosci. *7*, 358–366. https://doi.org/10.1038/nrn1888.

32. Wilson, D.E., Whitney, D.E., Scholl, B., and Fitzpatrick, D. (2016). Orientation selectivity and the functional clustering of synaptic inputs in primary visual cortex. Nat. Neurosci. *19*, 1003–1009. https://doi.org/10.1038/nn.4323.

33. Lee, K.F.H., Soares, C., Thivierge, J.-P., and Béïque, J.-C. (2016). Correlated Synaptic Inputs Drive Dendritic Calcium Amplification and Cooperative Plasticity during Clustered Synapse Development. Neuron *89*, 784–799. https://doi.org/10.1016/j.neuron.2016.01.012.

34. Scholl, B., Wilson, D.E., and Fitzpatrick, D. (2017). Local Order within Global Disorder: Synaptic Architecture of Visual Space. Neuron *96*, 1127–1138.e4. https://doi.org/10.1016/j.neuron.2017.10.017.

35. Kerlin, A., Mohar, B., Flickinger, D., MacLennan, B.J., Dean, M.B., Davis, C., Spruston, N., and Svoboda, K. (2019). Functional clustering of dendritic activity during decision-making. eLife *8*, e46966. https://doi.org/10.7554/eLife.46966.

36. Hedrick, N.G., Lu, Z., Bushong, E., Singhi, S., Nguyen, P., Magaña, Y., Jilani, S., Lim, B.K., Ellisman, M., and Komiyama, T. (2022). Learning binds new inputs into functional synaptic clusters via spinogenesis. Nat. Neurosci. *25*, 726–737. https://doi.org/10.1038/s41593-022-01086-6.

37. Noguchi, J., Nagaoka, A., Watanabe, S., Ellis-Davies, G.C.R., Kitamura, K., Kano, M., Matsuzaki, M., and Kasai, H. (2011). In vivo two-photon uncaging of glutamate revealing the structure-function relationships of dendritic spines in the neocortex of adult mice. J. Physiol. *589*, 2447–2457. https://doi.org/10.1113/jphysiol.2011.207100.

38. Lee, W.-C.A., Bonin, V., Reed, M., Graham, B.J., Hood, G., Glattfelder, K., and Reid, R.C. (2016). Anatomy and function of an excitatory network in the visual cortex. Nature *532*, 370–374. https://doi.org/10.1038/nature17192.

39. Hagihara, K.M., Murakami, T., Yoshida, T., Tagawa, Y., and Ohki, K. (2015). Neuronal activity is not required for the initial formation and maturation of visual selectivity. Nat. Neurosci. *18*, 1780–1788. https://doi.org/10.1038/nn.4155.

40. Lien, A.D., and Scanziani, M. (2013). Tuned thalamic excitation is amplified by visual cortical circuits. Nat. Neurosci. *16*, 1315–1323. https://doi.org/10.1038/nn.3488.

41. Scholl, B., Tan, A.Y.Y., Corey, J., and Priebe, N.J. (2013). Emergence of Orientation Selectivity in the Mammalian Visual Pathway. J. Neurosci. *33*, 10616–10624. https://doi.org/10.1523/JNEUROSCI.0404-13.2013.

42. Sun, W., Tan, Z., Mensh, B.D., and Ji, N. (2016). Thalamus provides layer 4 of primary visual cortex with orientation- and direction-tuned inputs. Nat. Neurosci. *19*, 308–315. https://doi.org/10.1038/nn.4196.

43. Balcioglu, A., Gillani, R., Doron, M., Burnell, K., Ku, T., Erisir, A., Chung, K., Segev, I., and Nedivi, E. (2023). Mapping thalamic innervation to individual L2/3 pyramidal neurons and modeling their 'readout' of visual input. Nat. Neurosci. *26*, 470–480. https://doi.org/10.1038/s41593-022-01253-9.

44. Letzkus, J.J., Kampa, B.M., and Stuart, G.J. (2006). Learning Rules for Spike Timing-Dependent Plasticity Depend on Dendritic Synapse Location. J. Neurosci. *26*, 10420–10429. https://doi.org/10.1523/JNEUROSCI.2650-06.2006.

45. Park, J., Papoutsi, A., Ash, R.T., Marin, M.A., Poirazi, P., and Smirnakis, S.M. (2019). Contribution of apical and basal dendrites to orientation encoding in mouse V1 L2/3 pyramidal neurons. Nat. Commun. *10*, 5372. https://doi.org/10.1038/s41467-019-13029-0.

46. Ju, N., Li, Y., Liu, F., Jiang, H., Macknik, S.L., Martinez-Conde, S., and Tang, S. (2020). Spatiotemporal functional organization of excitatory synaptic inputs onto macaque V1 neurons. Nat. Commun. *11*, 697. https://doi.org/10.1038/s41467-020-14501-y.

47. Chen, W., Ge, X., Zhang, Q., Natan, R.G., Fan, J.L., Scanziani, M., and Ji, N. (2024). High-throughput volumetric mapping of synaptic transmission. Nat. Methods *21*, 1298–1305. https://doi.org/10.1038/s41592-024-02309-3.

48. Okuno, H., Akashi, K., Ishii, Y., Yagishita-Kyo, N., Suzuki, K., Nonaka, M., Kawashima, T., Fujii, H., Takemoto-Kimura, S., Abe, M., et al. (2012). Inverse synaptic tagging of inactive synapses via dynamic interaction of Arc/Arg3.1 with CaMKIIβ. Cell *149*, 886–898. https://doi.org/10.1016/j.cell.2012.02.062.

49. De Roo, M., Klauser, P., and Muller, D. (2008). LTP Promotes a Selective Long-Term Stabilization and Clustering of Dendritic Spines. PLoS Biol. *6*, e219. https://doi.org/10.1371/journal.pbio.0060219.

50. Kleindienst, T., Winnubst, J., Roth-Alpermann, C., Bonhoeffer, T., and Lohmann, C. (2011). Activity-dependent clustering of functional synaptic inputs on developing hippocampal dendrites. Neuron *72*, 1012–1024. https://doi.org/10.1016/j.neuron.2011.10.015.

51. Takahashi, N., Kitamura, K., Matsuo, N., Mayford, M., Kano, M., Matsuki, N., and Ikegaya, Y. (2012). Locally Synchronized Synaptic Inputs. Science *335*, 353–356. https://doi.org/10.1126/science.1210362.

52. Tazerart, S., Mitchell, D.E., Miranda-Rottmann, S., and Araya, R. (2020). A spike-timing-dependent plasticity rule for dendritic spines. Nat. Commun. *11*, 4276. https://doi.org/10.1038/s41467-020-17861-7.

53. Chen, X., Leischner, U., Rochefort, N.L., Nelken, I., and Konnerth, A. (2011). Functional mapping of single spines in cortical neurons in vivo. Nature *475*, 501–505. https://doi.org/10.1038/nature10193.

54. Palmer, L., Murayama, M., and Larkum, M. (2012). Inhibitory Regulation of Dendritic Activity in vivo. Front. Neural Circuits *6*, 26. https://doi.org/10.3389/fncir.2012.00026.

55. Marvin, J.S., Shimoda, Y., Magloire, V., Leite, M., Kawashima, T., Jensen, T.P., Kolb, I., Knott, E.L., Novak, O., Podgorski, K., et al. (2019). A genetically encoded fluorescent sensor for in vivo imaging of GABA. Nat. Methods *16*, 763–770. https://doi.org/10.1038/s41592-019-0471-2.

56. Chen, J.L., Villa, K.L., Cha, J.W., So, P.T.C., Kubota, Y., and Nedivi, E. (2012). Clustered Dynamics of Inhibitory Synapses and Dendritic Spines in the Adult Neocortex. Neuron *74*, 361–373. https://doi.org/10.1016/j.neuron.2012.02.030.

57. Tseng, Q., Wang, I., Duchemin-Pelletier, E., Azioune, A., Carpi, N., Gao, J., Filhol, O., Piel, M., Théry, M., and Balland, M. (2011). A new micropatterning method of soft substrates reveals that different tumorigenic signals can promote or reduce cell contraction levels. Lab Chip *11*, 2231–2240. https://doi.org/10.1039/c0lc00641f.

58. Rikhye, R.V., Yildirim, M., Hu, M., Breton-Provencher, V., and Sur, M. (2021). Reliable Sensory Processing in Mouse Visual Cortex through Cooperative Interactions between Somatostatin and Parvalbumin Interneurons. J. Neurosci. *41*, 8761–8778. https://doi.org/10.1523/JNEUROSCI.3176-20.2021.

59. Mazurek, M., Kager, M., and Van Hooser, S.D. (2014). Robust quantification of orientation selectivity and direction selectivity. Front. Neural Circuits *8*, 92. https://doi.org/10.3389/fncir.2014.00092.

60. Aarts, E., Verhage, M., Veenvliet, J.V., Dolan, C.V., and Van Der Sluis, S. (2014). A solution to dependency: using multilevel analysis to accommodate nested data. Nat. Neurosci. *17*, 491–496. https://doi.org/10.3389/fncir.2014.00092.

## STAR★METHODS

### KEY RESOURCES TABLE

| REAGENT or RESOURCE | SOURCE | IDENTIFIER |
|---|---|---|
| Bacterial and virus strains | | |
| AAV9-CaMKII 0.4.Cre-SV40 | Addgene | 105558-AAV9 |
| AAV1-hSyn1-Flex-mRuby2-GSG-P2A-GCaMP6s-WPRE-pA | Addgene | 68720-AAV1 |
| Deposited data | | |
| Original code | This paper | Zenodo: https://doi.org/10.5281/zenodo.18552067 |
| Original data | This paper | Zenodo: https://doi.org/10.5281/zenodo.19372968 |
| Experimental models: Organisms/strains | | |
| C57BL/6J | The Jackson Laboratory | 000664 |
| Software and algorithms | | |
| MATLAB | Mathworks | R2024b |
| Neurolucida | MBF Bioscience | 2020 |

### EXPERIMENTAL MODEL AND STUDY PARTICIPANT DETAILS

All procedures detailed in the STAR Methods were approved by the Massachusetts Institute of Technology's Animal Care and Use Committee (protocol number 2308000562) and conformed to NIH guidelines. Both male and female C57BL/6J (JAX000664) mice born in our animal colony were used. Mice were group housed with littermates post weaning (no more than 5 per cage) but single housed following surgery. All mice had a standard light/dark 12/12-hour cycle with an average temperature of 21°C and average humidity of 50%. All recordings were done during the light cycle. The mice had access to food and water *ad libitum*. Details for each experimental subject, including age at time of the experiment and sex, are listed in Table 1.

### METHOD DETAILS

#### Surgical preparation

Experiments were performed in adolescent and adult mice (> postnatal day (P)33). Animals were anesthetized with isoflurane (2%), and pre-surgical slow-release buprenorphine (1 mg/kg) and meloxicam (5 mg/kg) were administered subcutaneously. The mice were placed on a Kopf stereotax with their body temperature maintained using a heating pad (ATC2000, World Precision Instruments). Fur was removed from the scalp using Nair. 0.1 mLs of bupivacaine (0.5%) was injected locally, and the scalp was cleaned by 3 alternating applications of betadine and 70% ethanol. After confirming the appropriate level of anesthesia, the skin over the scalp was removed using iris scissors to expose an area of the skull roughly encompassing the frontal and interparietal bone widths. After leveling, the skull was scraped clean and scored with a scalpel. A 3 mm circle was outlined on the left hemisphere 1 mm anterior and 3 mm lateral to the intersection of the Lambda and midline sutures. A circular craniotomy was then performed while frequently wetting the skull with ice cold mammalian Ringer's solution (50-980-245, Fisher Scientific), until the circular bone fragment could be easily lifted off under a drop of Ringer's. A mixture of AAV9-CaMKII 0.4.Cre-SV40 (~3e7-e8 vg/mL, 105558-AAV9, Addgene) and AAV1-hSyn1-Flex-mRuby2-GSG-P2A-GCaMP6s-WPRE-pA (~5e12 vg/mL, 68720-AAV1, Addgene) diluted in Ringer's solution was injected (QSI 53311, Stoelting) through a pulled glass pipette with a beveled 50 μm opening 0.2-0.4 mm below the dura at 3-4 locations spaced >0.5 mm apart. Injection sites were confined to 2.5-3.5 mm lateral and 0-1 mm anterior the intersection of the Lambda and midline sutures to target the binocular region of the left visual cortex (V1). 150 nL was injected per site at a rate of 50 nL/min. The craniotomy was then sealed with a stack of two 3 mm circular coverslips and a 5 mm circular coverslip (CS-3R and CS-5R #1 thickness, Warner Instruments) previously glued together with optical adhesive (NOA 61, Norland), which compressed the cortex improving imaging stability. The edges of the 5 mm coverslip and exposed skull were then covered with Metabond (C&B Metabond, Parkell) mixed with black ink pigment (Black Iron Oxide 18727, Schmincke) to minimize light leak. Finally, a custom designed stainless steel headplate (eMachine Shop) was positioned over the cranial window and fixed in place using additional Metabond. Animals were allowed to recover from anesthesia, placed in a clean cage, and supplemented with heat, saline, and additional meloxicam as needed during a 3-day recovery window. Imaging began no sooner than two weeks following window implantation.

A subset of the mice in this study (N=5 mice, n = 5 neurons) were used in a previous publication[5] but the analyses are reported here for the first time. These mice were prepared as described above, with the exception that the injection of virus was performed through the skull in a separate surgery at ~P9, after which the skin was sutured (Prolene 7.0, Ethicon) and the mouse returned to the dam cage. The placement of the window was performed as detailed above in a subsequent surgery at ~P20. All data reported from all mice in this study were collected after P33.

### Two-photon imaging

All imaging was performed on a Prairie Ultima IV (Bruker) two-photon microscope using resonant galvo scanning at 512x512 pixels, 15.15-25.00 pixels/μm, and 920 nm excitation with a tunable laser (MaiTai eHP, Spectra Physics). Due to the low signal inherent in dendritic spine imaging, data was acquired using 4-frame averaging leading to an effective imaging rate of ~7.75 Hz. All imaging was performed using an XLPlan N 20x 1.00 NA or 25x 1.05NA (Olympus) objective. The emission light was split by a dichroic and further filtered to collect red (mRuby2, 590/50 nm) and green (GCaMP6s, 525/50 nm) light separately with GaAsP PMTs (H7422PA-40, Hamamatsu). To synchronize image acquisition with visual stimuli, an analog 5-volt pulse was generated for every stimulus shown via a data acquisition device (BNC-2110, National Instruments) and recorded at 1 KHz by an analog to digital converter to the same software controlling image acquisition (Prairieview, Bruker). Imaged neurons were selected based on the depth of their soma (greater than 100 μm from the surface), the presence of an apical dendrite extending upwards into layer 1, and a qualitative assessment of the level of viral expression. Neurons displaying over-expression (characterized by frequent, large-scale depolarizations and GCaMP6s expression in the nucleus) or under-expression (signal too low to reliably track distal dendrites or resolve individual spines) were not selected for imaging or discarded during subsequent quality control. Additionally, some neurons that were too close to a neighboring neuron to reliably distinguish their processes were discarded. The soma and multiple sections of dendrite were imaged in separate recordings (non-simultaneously). Dendrites with long stretches running parallel to the imaging plane, and thus in focus, were selected for imaging. The location of each dendritic field of view was manually annotated for later alignment to a structural Z-scan of the dendritic arbor, which was acquired at the end of functional imaging with 1010 nm excitation and digital magnification sufficient to capture all imaged fields of view.

Mice were habituated to an imaging rig, which consisted of a metal bar to which the headplate was affixed, a polypropylene tube to constrain movement, moveable eye-blockers, and an LCD monitor (11.6-inch, 60 Hz refresh rate, LONCEVON) centered 9 cm in front of the mouse perpendicular to the visual field extending ~100° in azimuth and ~60° in elevation, with a mean luminance of 35 cd/m$^2$. Light from the monitor was kept from the objective using a custom light blocker attached to the headplate and draped over the imaging rig. All neuronal and spine responses reported here were measured with binocular visual stimulation. 2-3 fields of view were imaged per mouse per day with additional fields of view taken on subsequent days. Mice viewed drifting sinusoidal grating (0.02-0.08 cycles per degree, 2 Hz temporal frequency) in 22.5-45° intervals, with each direction repeated 10 times for 1 second per repetition in pseudorandom order with 3-4 second interstimulus interval times in which a gray screen was shown.

### Image processing and ROI selection

Individual TIFF image files for both the red and green channel were separately concatenated. For fields of view with separate recordings performed for the ipsilateral eye, contralateral eye, and binocular viewing, the TIFF stacks from each recording were then concatenated. Motion correction was performed in FIJI using the Template-Matching plugin,[57] with two rounds of motion correction, the first round aligned to the first frame of imaging and the second round aligned to the average intensity projection of all frames. Only the central 312x312 pixels were used for determining registration. The XY frame shifts from each round were recorded in csv files. In some cases where motion was overcorrected or under-corrected, registration was re-run by selecting a different frame for the initial registration or using an average intensity projection from a stable section of the recording. If motion remained too high to reliably estimate spine boundaries, the field of view was discarded. The average intensity projection of the registered stack was then used for region of interest (ROI) selection. For dendritic imaging, spines were manually selected using the ImageJ polygon or circular selection tool. For each spine, an equivalently shaped nearby area of background not containing any processes was selected (for control measurements of dark noise and light leak) as well as a polygonal section of the adjacent dendritic shaft for later signal correction. For soma imaging, the polygon selection tool was used to select the soma and an adjacent area of background. The drawn ROIs in all cases were used to extract the mean pixel intensity per ROI per frame and saved as a CSV file for later analysis.

### Functional analysis for two-photon imaging data

All subsequent functional analysis was performed in MATLAB. For somata, the signal from the background ROI was subtracted from the somatic ROI to remove noise prior to z-scoring the trace using the mean and standard deviation of the concatenated last halves of each interstimulus interval period. For spines, the trace for both the raw spine and its adjacent dendritic shaft were $(F-F_0)/F_0$ transformed using the mean fluorescence ($F_0$) taken during the concatenated last halves of each interstimulus interval period. To remove shared signal between the spine and the dendritic shaft, a robust fit was then performed between the shaft and the spine and the resulting coefficient used to subtract the scaled shaft signal from the spine signal.[2] This corrected spine signal was z-scored using the mean and standard deviation of the concatenated last halves of each interstimulus interval period.

Frame timestamps were aligned to the beginning of each unique visual stimulus using the analog 5-volt signal generated during recording, with the start of each stimulus set to time 0. For each soma/spine, the response to each repetition of a unique stimulus

was then linearly interpolated to 10 Hz to align responses relative to the stimulus start time. Mean activity was computed for each repetition both pre-stimulus (-2 to 0 seconds) and post-stimulus (0-1 seconds) and the post-pre difference taken as the amplitude of each trial. For somas and spines, trials with a pre-stimulus mean >2 (analogous to >2 standard deviations above the mean) were excluded. In addition, for spines, the mean was taken of all dendritic shaft ROIs' fluorescence and trials in which this average dropped below 2 standard deviations of the mean were excluded as trials presumably with high motion artifact. A threshold of >2 standard deviations from the mean for the dendritic shaft (lasting at least 2 frames) was also used to count the number of back propagating action potentials for each dendritic segment, and this number was normalized within each neuron across its dendritic segments to determine the effect of distance from soma and branch type.

We defined the preferred stimulus for each soma or spine as the grating direction that elicited the maximum median response amplitude. For both somata and spines, a time-series Zeta test[25] was used to determine if the soma/spine was significantly responsive to its preferred stimulus (parameters: duration = stimulus duration, jitter = interstimulus interval duration, repetitions = 1000, significance level = 0.05, Version 1.0). Only somata/spines significantly responsive to their preferred stimulus were labeled as responsive, to avoid multiple comparisons from testing responsiveness to each direction of drifting grating separately.

The reliability index was computed as the mean pairwise correlation between trials for the soma or spine's preferred stimulus.[58] Orientation and direction tuning were computed using a vector based approach.[59] Using the median trial amplitudes for all directions, direction selectivity was calculated as $\mathrm{DSI} = \frac{abs\left(\left(\sum_k R(\theta k)\exp(i\theta k)\right)\right)}{\sum_k R(\theta k)}$, where $R(\theta k)$ is the response to direction $\theta k$. After averaging the responses to opposite directions, OSI was calculated as $\mathrm{OSI} = \frac{abs\left(\left(\sum_k R(\theta k)\exp(2i\theta k)\right)\right)}{\sum_k R(\theta k)}$, where $R(\theta k)$ is the response to orientation $\theta k$. The mean orientation preference for spines included in a given analysis was calculated as $\alpha = angle\left(\frac{1}{k}\sum_k \exp\left(2i\theta k\right)\right)$ where $\theta k$ is the preferred orientation of a spine and there are $k$ spines. Orientation dispersion was then calculated as the mean distance of the spines' orientation preference from the mean orientation preference, as $\frac{1}{2k}\sum_k \pi - |\pi - |2\theta k - \alpha||$. For pairs of spines and for each spine to its parent soma, the tuning correlation was computed as the Pearson's correlation between the vector of their median trial amplitude to each stimulus. Summed input was calculated as the sum, for each stimulus, of all responsive spines' median trial amplitude in z-scored units. This is equivalent to the sum of the median trial amplitude tuning curves of all (recorded) responsive spines.

### Structural analysis of two-photon imaging data

Spine size was computed for each ROI using the vertices of the ROI drawn in ImageJ and the MATLAB polyarea function. Fields of view were manually annotated as apical or basal based upon the neuron's morphology. Pairwise spine distances were computed within a field of view by first tracing the dendritic segment in ImageJ, with separate traces in the case of fields of view with multiple branches or branch points. The intersection point of each spine with the traced dendrite was then computed. For each pair of spines, their pairwise distance was taken as the distance between their intersections along the traced dendrite. This allows for a more accurate estimation of distance relevant to the propagation of biological signals, such as voltage along the shaft, than does Euclidean distances between spine pairs themselves. For calculating distance from the soma for each dendritic field of view, the structural scan of each neuron was imported into Neurolucida (MBF Bioscience), the apical dendrite and basal dendrites were traced, and the imaged field of views mapped to the reconstructed neuron based on the morphology, depth, and manual annotation performed during imaging. Fields of view in which the location in the dendritic arbor could not be accurately gauged were not assigned a distance from the soma but were still used in all other analyses not requiring distance from soma. In analyses in which the distance from soma was required, only neurons and fields of view with a known distance from the soma were included.

## QUANTIFICATION AND STATISTICAL ANALYSIS

The statistics used and degrees of freedom in each analysis are reported in the figure captions, significant results are identified with an asterisk, and Table 1 summarizes the technical and biological variables of each mouse and neuron. All statistics were performed in MATLAB. Both male and female mice were used.

Statistics where N is number of neurons: For comparisons where a single average is taken across each neuron's spines and groups of neurons compared (e.g. responsive vs. unresponsive neurons), a two-sided two-sample *t*-test was used. For comparisons of means from different groups of spines within a neuron, such as between apical and basal, a two-sided paired *t*-test was used. Partial correlations were calculated for each neuron independently, and then a one-sample *t*-test used to test the partial correlations of the group of neurons against the null hypothesis of a mean partial correlation of 0. For correlation between a somatic response property, such as OSI, and an averaged or summed spine property, the Rho and p-value was computed for the Pearson's correlation using a *t*-distribution.

Statistics where N is number of dendritic spines: For comparisons of a spine property within or between groups, an analysis of variance (ANOVA) for linear mixed-effects model was used with the identity of each spine's parent neuron as a random effect. This was to account for the interdependence of spines measured from the same neuron.[60] Neuron identity was modeled as a random effect as opposed to the experimental subject identity as only one neuron was recorded from most mice (16/19 mice).

Clustering analysis: Analysis of clustering was only performed for fields of view that had 4 or more responsive spines to allow for randomization tests within the field of view. For the randomization tests, the field of view's pairwise distances for responsive spines were randomized using either all pairs of spines or only the responsive pairs of spines, separately shuffled 10,000 times. For responsive spine clustering, the median pairwise responsive-responsive distance was compared to the distribution of the medians of the shuffled pairwise distances for all pairs and had to be outside the 0.025-0.975 percentile of the shuffled distribution to reach significance. For distance-dependent tuning correlation, the pairwise correlations for responsive spine pairs were binned in 5 μm increments using their original pairwise distances and each of the 10,000 shuffles of the responsive-responsive spine pairs' distances. To determine the significance of the original data versus the shuffled data in each bin, the mean correlation for each bin was compared to the distribution of mean correlations for the shuffles and had to be outside the 0.025-0.975 percentile of the shuffled means to reach significance for that bin. To split spines into proximal and distal, for each neuron we separately took the median distances from soma for the apical segments and the basal segments to split them into the 50% most proximal and 50% most distal while maintaining the balance between apical and basal segments from the original data. In the case of an odd number of apical or basal segments, the median segment was discarded.

Linear mixed effect model with multiple predictors: Based on our analysis of clustering, the tuning correlation between a responsive spine and its nearest responsive neighbor was only included in the model as a predictor if they were <5 μm apart. In addition, we normalized each spine's correlation to its nearest neighbor by its mean correlation to all other spines on that neuron, as correlation to the soma and mean pairwise correlation are themselves correlated due to the underlying bias for the soma's preferred stimulus.

Non-categorical variables were z-scored separately in tables containing either all responsive spines or containing only responsive spines from fields of view with a known distance from the soma. 10,000 repetitions of five-fold cross validation were then run, with partitions maintaining similar proportions of spines from each neuron as in the non-partitioned data. For each repetition/fold, a linear mixed-effects model was run for each predictor alone, combinations of all but one predictor, and the full model of all predictors on 4 of the 5 folds (training data) with each fold being held-out once. For individual predictor models, the coefficient and lower/upper bounds were taken and the medians reported. For leave-one-out models and the full model, the R-squared ($R^2$) values were computed by applying the trained model from each repetition/fold to the held-out fold (test data) to calculate the sum of the squared residuals (SSE) and the total sum of squares (TSS), with:

$$R^2 = 1 - \left(\frac{SSE_{test}}{TSS_{test}}\right)$$

For each of the leave-one-out models, the difference in $R^2$ was taken from the full model's $R^2$ to calculate the explained variance from the left-out predictor. The mean difference was then taken across the five folds for each of the repetitions to give a distribution allowing the median and range of variance explained to be visualized, and a one-sided bootstrap analysis across the repetitions used to compute a distribution for determining significance based on explained variance being >0, corrected for multiple comparisons (the number of leave one out models being tested). For distance from soma, the data used only included fields of view with known distance from the soma. The full linear mixed-effects model (including distance from the soma) in Wilkinson notation was:

$$Corr_{n,i} \sim 1 + osi_i + dsi_i + rel_i + s_i + wc_i + ab + d_i + (1|n)$$

where $corr_{n,i}$ is the tuning correlation of spine $i$ on neuron $n$ to the soma, $osi_i$ is the OSI of spine $i$, $dsi_i$ is the DSI of spine $i$, $rel_i$ is the reliability of spine $i$ to its preferred stimulus, $s_i$ is the size of spine $i$, $wc_i$ is spine $i$'s normalized correlation to its nearest neighbor (or 0 if no other responsive spine was within 5 μm), $ab$ is a categorical variable signifying whether spine $i$ is apical or basal, $d_i$ is spine $i$'s distance from the soma, and $(1|n)$ is a random effect of neuron $n$ on the y-intercept.